Mon. Not. R. Astron. Soc. **353,** 624–632 (2004) doi:10.1111/j.1365-2966.2004.08094.x

Convergence and scatter of cluster density profiles

Jürg Diemand,★ Ben Moore and Joachim Stadel

Institute for Theoretical Physics, University of Zürich, Winterthurerstrasse 190, CH-8057 Zürich, Switzerland

Accepted 2004 June 2. Received 2004 May 28; in original form 2004 February 11

ABSTRACT

We present new results from a series of ΛCDM simulations of cluster mass haloes resolved with high force and mass resolution. These results are compared with recently published simulations from groups using various codes including PKDGRAV, ART, TPM, GRAPE and GADGET. Careful resolution tests show that with 25 million particles within the high-resolution region we can resolve to about 0.3 per cent of the virial radius and that convergence in radius is proportional to the mean interparticle separation. The density profiles of 26 high-resolution clusters obtained with the different codes and from different initial conditions agree very well. The average logarithmic slope at one per cent of the virial radius is $\gamma = 1.26$ with a scatter of ± 0.17. Over the entire resolved regions the density profiles are well fitted by a smooth function that asymptotes to a central cusp $\rho \propto r^{-\gamma}$, where we find $\gamma = 1.16 \pm 0.14$ from the mean of the fits to our six highest-resolution clusters.

Key words: methods: *N*-body simulations – methods: numerical – galaxies: clusters: general – galaxies: haloes – dark matter.

1 INTRODUCTION

A highly motivated and well-defined problem in computational astrophysics is to compute the non-linear structure of dark matter haloes. This is especially timely given the abundance of new high-resolution data that probe the central structure of galaxies (e.g. de Blok et al. 2001a; de Blok, McGaugh & Rubin 2001b; McGaugh, Rubin & de Blok 2001; de Blok & Bosma 2002; Swaters et al. 2003) and clusters (e.g. Sand et al. 2004). Furthermore, a standard cosmological paradigm has been defined that gives a well-defined framework within which to perform numerical calculations of structure formation (e.g. Spergel et al. 2003). This subject has developed rapidly over the past few years, building upon the pioneering results obtained in the early 1990s by Dubinski & Carlberg (1991) and Warren et al. (1992). More recently, the systematic study of many haloes at low resolution led to the proposal that cold dark matter haloes could all be fit by a universal two-parameter function (Navarro, Frenk & White 1996, hereafter NFW), with a slope of r^{-1} at one per cent of the virial radius. At the same time, the study of a few haloes at high-resolution questioned these results (Fukushige & Makino 1997; Moore et al. 1998, 1999, hereafter M99; Ghigna et al. 2000; Jing & Suto 2000). These latter authors claimed that of order a million particles within the virialized region where necessary to resolve the halo structure to 1 per cent and the slopes at that radius could be significantly steeper. Just within the last few months, we have seen several groups publish reasonably large samples of haloes simulated with the necessary resolution that we can finally determine the scatter in the density profiles across a range of mass scales (Fukushige, Kawai & Makino 2004, hereafter F04; Hayashi et al. 2003, hereafter H03; Navarro et al. 2004; Reed et al. 2003; Tasitsiomi et al. 2004, hereafter T04; Wambsganss, Bode & Ostriker 2004, hereafter W04).

Much of the recent controversy in the literature has been due to limited statistics and the lack of agreement over what is a reliable radius for trusting a given simulation with a given set of parameters. Several studies have attempted to address this issue (Moore et al. 1998; Knebe et al. 2000; Klypin et al. 2001; Power et al. 2003; Diemand et al. 2004). Integration and force accuracy can be understood using controlled test simulations. However, discreteness is probably the most important and least understood numerical effect that can influence our numerical results, and it is exacerbated owing to the lack of an analytic solution with which to compare simulations. Our particle sampling of the nearly collisionless fluid we attempt to simulate can lead to energy transfer and mass redistribution, particularly in the central regions that we are often most interested in.

Collisional effects in the final object or in the early hierarchy of objects can be reduced by increasing the number of particles N in a simulation (Diemand et al. 2004). The limitation to the phase space densities that can be resolved due to discreteness in the initial conditions can also be overcome by increasing the resolution (Binney 2004). As we increase the resolution within a particular non-linear structure, we find that the global properties of the resolved structure is retained, including shape, density profile, substructure mass functions and even the positions of the infalling substructures. This gives us confidence that our N-body calculations are not biased by using finite N (Baertschiger, Joyce & Sylos Labini 2002). The fact that increasing the resolution allows us to resolve smaller radii is

★E-mail: diemand@physik.unizh.ch

Table 1. Parameters of simulated cluster haloes.

Run	z_i	ϵ_0 (kpc)	$\epsilon_{\max}$ (kpc)	$N_{\rm vir}$	$M_{\rm vir}$ $\times 10^{15}$ ($M_\odot$)	$r_{\rm vir}$ (kpc)	$Vc_{\max}$ (km s^{-1})	$r_{\max}$ (kpc)	$r_{\rm resolved}$ (kpc)
*A*9	40.27	2.4	24	24 987 606	1.29	2850	1428	1853	9.0
*B*9	40.27	4.8	48	11 400 727	0.59	2166	1120	1321	14.4
*C*9	40.27	2.4	2.4	9 729 082	0.50	2055	1090	904	9.0
*D*3*h*	29.44	1.8	18	205 061	0.28	1704	944	834	27
*D*6*h*	36.13	1.8	18	1 756 313	0.31	1743	975	784	13.5
*D*6	36.13	3.6	36	1 776 849	0.31	1749	981	840	13.5
*D*9	40.27	2.4	24	6 046 638	0.31	1752	983	876	9.0
*D*9*lt*	40.27	2.4	24	6 036 701	0.31	1752	984	841	9.0
*D*12	43.31	1.8	18	14 066 458	0.31	1743	958	645	6.8
*E*9	40.27	2.4	24	5 005 907	0.26	1647	891	889	9.0
*F*9	40.27	2.4	24	4 567 075	0.24	1598	897	655	9.0
*F*9*cm*	40.27	2.4	2.4	4 566 800	0.24	1598	898	655	9.0
*F*9*ft*	40.27	2.4	99.06	4 593 407	0.24	1601	905	464	9.0

important since the baryons often probe just the central few per cent of a dark matter structure – the latest observations of galaxies and clusters probe the mass distribution within one per cent of the virial radius, which until recently was unresolved by numerical simulations. Forthcoming experiments, such as VERITAS (Weekes et al. 2002) and MAGIC (Flix, Martinez & Prada 2004) will probe the structure of dark matter haloes on even smaller scales by attempting to detect gamma-rays from dark matter annihilation within the central hundred parsecs ($\sim$0.1 per cent $R_{\rm virial}$) of the Galactic halo (Calcaneo-Roldan & Moore 2000).

A simple estimate of the scaling of N with time shows remarkable progress over and above that predicted by Moore's law. The first computer simulations used of the order of 10^2 particles and force resolutions of the order of the half mass radii (Peebles 1970). Today we can follow up to 10^8 particles with a resolution of 10^{-3} of the final structure. The increase in resolution is significantly faster than predicted by Moore's law since equally impressive gains in performance have been due to advances in software.

We are finally at the stage whereby dark matter clustering is understood at a level where the uncertainties are dominated by the influence of the baryonic component. It is therefore a good time to review and compare existing results from different groups together with a set of new simulations that we have carried out that are the state of the art in this subject and represent what is achievable with several months of dedicated supercomputer time. For certain problems, such as predicting the annihilation flux discussed earlier, it would be necessary significantly to increase the resolution. This is not possible with existing resources and new techniques should be explored. We begin by presenting our new simulations in Section 2. Section 3 discusses convergence tests and the asymptotic best-fit density profiles. In Section 4 we compare our results with recently published results from four other groups mentioned above.

2 NUMERICAL EXPERIMENTS

Table 1 gives an overview of the simulations we present in this paper. With up to 25×10^6 particles inside the virial radius of a cluster and an effective 10^5 time-steps, they are among the highest-resolution ΛCDM simulations performed so far. They represent a major investment of computing time, the largest run was completed in about 10^5 CPU hours on the zBox supercomputer.[1]

[1] http://www-theorie.physik.unizh.ch/~stadel/zBox/

2.1 *N*-body code and numerical parameters

The simulations have been performed using a new version of PKDGRAV, written by Joachim Stadel and Thomas Quinn (Stadel 2001). The code was optimized to reduce the computational cost of the very-high-resolution runs we present in this paper. We tested the new version of the code by rerunning the 'Virgo cluster' initial conditions (Moore et al. 1998). We confirmed that density profile, shape of the cluster and the amount of substructure it contains is identical with that obtained with the original code presented in Ghigna et al. (1998).

Individual time-steps are chosen for each particle proportional to the square root of the softening length over the acceleration, $\Delta t_i = \eta\sqrt{\epsilon/a_i}$. We used $\eta = 0.2$ for most runs, only in run *D*9*lt* we used larger time-steps $\eta = 0.3$ for comparison. The node-opening angle is set to $\theta = 0.55$ initially, and after $z = 2$ to $\theta = 0.7$. This allows higher force accuracy when the mass distribution is nearly smooth and the relative force errors can be large in the treecode. Cell moments are expanded to fourth order in PKDGRAV, other treecodes typically use just second- or first-order expansion. The code uses a spline softening length ϵ; forces are completely Newtonian at 2ϵ. In Table 1, ϵ_0 is the softening length at $z = 0$, $\epsilon_{\max}$ is the maximal softening in comoving coordinates. In most runs, the softening is constant in physical coordinates from $z = 9$ to the present and is constant in comoving coordinates before, i.e. $\epsilon_{\max} = 10\,\epsilon_0$. In runs *C*9 and *F*9*cm* the softening is constant in comoving coordinates for the entire run, in run *F*9*ft* the softening has a constant physical length for the entire run.

2.2 Initial conditions and cosmological parameters

We adopt a ΛCDM cosmological model with parameters from the first year WMAP results: $\Omega_\Lambda = 0.732$, $\Omega_m = 0.268$, $\sigma_8 = 0.9$, $h = 0.71$ (Spergel et al. 2003). The initial conditions are generated with the GRAFIC 2 package (Bertschinger 2001). The starting redshifts z_i are set to the time when the standard deviation of the density fluctuations in the refined region reaches 0.2.

First we run a parent simulation: a 300^3 particle cubic grid with a comoving cube size of 300 Mpc (particle mass $m_{\rm p} = 3.7 \times 10^{10}$ $M_\odot$, force resolution $\epsilon_0 = 100$ kpc, $\epsilon_{\max} = 1$ Mpc). Then we use the friends-of-friends (FoF) algorithm (Davis et al. 1985) with a linking length of 0.164 mean interparticle separations to identify clusters.

We found 39 objects with virial masses above 2.3×10^{14} $M_\odot$. We selected six of these clusters for re-simulation, discarding objects close to the periodic boundaries and objects that show clear signs of recent major mergers at $z = 0$. We label the six clusters with letters *A* to *F* according to their mass. It turned out that two of the clusters selected in this way (runs *A* and *C*) have ongoing major mergers at $z = 0$ (i.e. two clearly distinguishable central cores), which is not evident from the parent simulation due to lack of resolution. These clusters were evolved slightly into the future to obtain a sample of six 'relaxed' clusters.

For re-simulation we trace back the particles within a cluster's virial radius to the initial conditions and add all particles within 4 Mpc of these to the refinement region. This ensures that there is no pollution of heavier particles within the virial radius of the re-simulated cluster. Typically one third or one quarter of the refinement particles end up within the virial radius. To reduce the mass differences at the border of the refinement region we define a 5-Mpc thick 'buffer region' around the high-resolution region, where an intermediate refinement factor of three or four in length is used. The final refinement factors are 6, 9 and 12 in length, i.e. 216, 729 and 1728 in mass, so that the mass resolution is $m_p = 2.14 \times 10^7$ $M_\odot$ in the highest-resolution run. We label each run with a letter indicating the object and number that gives the refinement factor in length. To reduce the mass differences at the border of the refinement region we define a 5-Mpc thick 'buffer region' around the high-resolution region, where an intermediate refinement factor of three or four in length is used.

2.3 Measuring density profiles

We define the virial radius $r_{\rm vir}$ such that the mean density within $r_{\rm vir}$ is 178 $\Omega_{\rm M}^{0.45} \rho_{\rm crit} = 98.4\ \rho_{\rm crit}$ for the adopted model (Eke, Cole & Frenk 1996). We use 30 spherical bins of equal logarithmic width, centred on the densest region of each cluster using TIPSY.[2] We confirmed that using triaxial bins adapted to the shape of the isodensity surfaces (at some given radius, we tried 0.1, 0.5 and $1 r_{\rm vir}$) does not change the form of the density profile, in agreement with Jing & Suto (2002). Binned profiles, and especially the slopes derived from them, are noisy; a kernel-based smoothing algorithm is presented in Reed et al. (2003). For simplicity and easier comparison with other results, we present only profiles obtained using spherical bins and without smoothing. Data points are plotted at the arithmetic mean of the corresponding bin boundaries; the first bin ends at 1.5 kpc, the last bin at the virial radius.

3 ΛCDM CLUSTER PROFILES

3.1 Profile convergence tests

Numerical convergence tests show that, with sufficient time-steps, force accuracy and force resolution, the radius a CDM simulation can resolve is limited by the mass resolution (Moore et al. 1998; Ghigna et al. 2000; Knebe et al. 2000; Klypin et al. 2001; F04; H03; Power et al. 2003; Reed et al. 2003). These tests compare different mass resolution simulations of the same object to determine the resolved radius. The resulting radii scale with $N^{-0.45}$ according to F04, H03 and Power et al. (2003), but only with $N^{-1/3}$ in the tests in Moore et al. (1998), Ghigna et al. (2000) and Reed et al. (2003).

[2] TIPSY is available form the University of Washington *N*-body group: http://www-hpcc.astro.washington.edu/tools/tipsy/tipsy.html

Table 2. Convergence radii measured by comparing with run *D*12. The numbers in the run labels are $\propto N^{1/3}$, at fixed force resolution we get $r \propto N^{-1/3}$ (bold values). Question marks indicate that a run with much better mass resolution than *D*12 would be needed to measure these convergence radii reliably. Stars indicate estimated radii assuming a convergence rate of $r \propto N^{-1/3}$.

Run	ϵ_0 (kpc)	$N_{\rm vir}$	$r_{10\,\rm per\,cent\,vc}$ (kpc)	$r_{10\,\rm per\,cent\,M}$ (kpc)	$r_{10\,\rm per\,cent\,\rho}$ (kpc)
*D*3*h*	1.8	205 061	**17.2**	**21.9**	**9.5**
*D*6*h*	1.8	1 756 313	**8.4**	**10.7**	**4.6**
*D*6	3.6	1 776 849	8.4	17.3	12.1
*D*9	2.4	6 046 638	3.2 ?	5.2 ?	2.2 ?
*D*9*lt*	2.4	6 036 701	5.2 ?	6.6 ?	2.8 ?
*D*9	2.4	6 046 638	5.7*	7.3*	3.2*
*D*12	1.8	14 066 458	4.2*	5.3*	2.4*

3.1.1 Mass resolution

The finite mass resolution of *N*-body simulations always leads to two-body relaxation effects, i.e. heat is transported into the cold halo cores and they expand. It is not obvious that better mass resolution reduces the effects of two-body relaxation, since in hierarchical models the first-resolved objects always contain just a few particles and with higher resolution these first objects form earlier, i.e. they are denser and more affected by relaxation effects (Moore 2001; Binney & Knebe 2002). Estimates of relaxation based on following the local phase-space density in simulations show that the amount of relaxation can be reduced with better mass resolution, but the average degree of relaxation scales roughly like $N^{-0.3}$, much slower than the N^{-1} expected from the relaxation time of the final structure (Diemand et al. 2004). This confirms the validity of performing convergence tests in *N*, but one has to bear in mind that convergence can be quite slow.

We checked a series of re-simulations of the same cluster (*D*) for convergence in circular velocity, mass enclosed[3] and density. Outside of the converged radii the values must be within 10 per cent of the reference run *D*12. Table 2 shows the measured converged radii.

(i) Convergence is slow, roughly $\propto N^{-1/3}$. Therefore a high-resolution reference run should have at least eight times as many particles. Between run *D*9 and *D*12 the factor is only 2.37. Using *D*12 to determine the converged radii of *D*9 gives radii that are about a factor two too small (Table 2). F04 compare runs with $N_{\rm vir} = 14 \times 10^6$ and $N_{\rm vir} = 29 \times 10^6$. At radii where both runs have similar densities it is still not clear if the simulations have converged; even higher-resolution studies are needed to demonstrate this.

(ii) If one sets the force resolution to one half of expected resolved radius, then it is not surprising to measure a resolved radius close to the expected value. With this method one can demonstrate almost arbitrary convergence criteria, as long as they overestimate $r_{\rm conv}$. Therefore convergence tests in *N* should be performed with small softenings (high force resolution). Runs *D*3*h*, *D*6*h* and *D*12 all have $\epsilon_0 = 1.8$ kpc; their converged radii scale as the mean interparticle separation $N^{-1/3}$. In run *D*6, $\epsilon_0 = 3.2$ kpc is close to the 'optimal value' from Power et al. (2003), and the converged radii are larger than in *D*6*h* (see Fig. 2).

[3] Convergence within 10 per cent in cumulative mass is the same as convergence in circular velocity with a tolerance of 5 per cent.

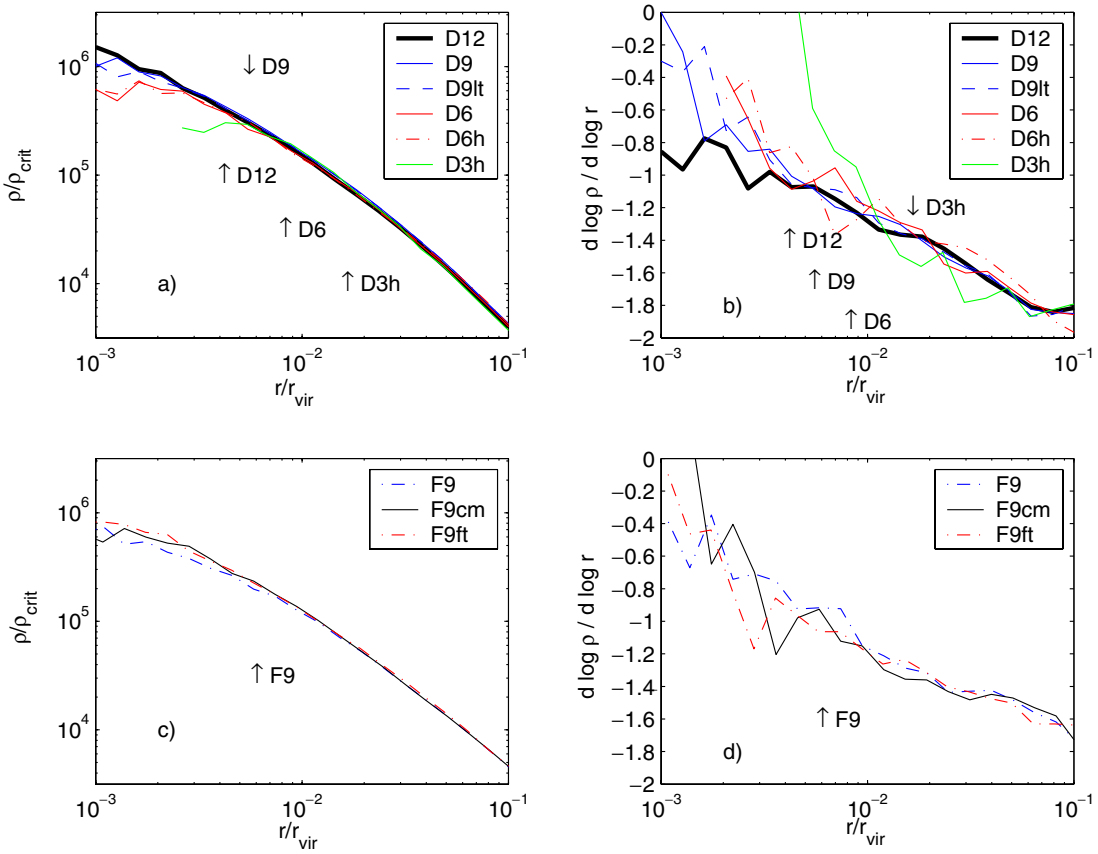

Figure 1. Numerical convergence tests for the cluster profiles. Panel (a): density profiles of cluster D resolved with $N_{\rm vir}$ = 205k, 1.8M, 6M and 14M particles. Panel (b): logarithmic slope for the profiles from (a). Panel (c): density profiles of cluster F simulated with different numerical parameters: $F9\,ft$ used 4096 fixed time-steps and constant ϵ in physical coordinates as in F04. $F9cm$ and $F9$ used adaptive time-steps $0.2\sqrt{\epsilon(z)/a}$ with comoving softening in $F9$ and mixed comoving/physical softening in $F9$ ($\epsilon_{\rm max} = 10\,\epsilon_0$). Panel (d): logarithmic slope for the profiles from (c).

(iii) Different small-scale noise in the initial conditions leads to different formation histories. Therefore the shape and the density profile can differ even at radii were all runs have converged. For example between $r = 10$ and 320 kpc, the densities in run $D9$ are about 7 per cent higher than in run $D12$. Therefore the densities in $D9$ are within 10 per cent of those of $D12$ quite early. If one re-scales ρ in this range $r_{10\,\rm per\,cent\,\rho}$ of $D9$ grows from 2.2 to 4.6 kpc.

Extrapolating $r_{\rm conv} \propto N^{-1/3}$ to our highest-resolution runs gives the values on the last two lines of Table 2. Note that this is just an extrapolation, it is not clear that this scaling is valid down to this level, only larger simulations could verify this. To be conservative we assume the limit due to mass resolution to be 9 kpc for the '9-series' of runs, and 6.8 kpc for run $D12$. The force resolution sets another limit at about $3\,\epsilon_0$. We give the larger of the two limits as the trusted radius in Table 1.

3.1.2 *Force and time resolution*

Finite time-steps and force resolution also sets a limiting radius/density that a run can resolve. We use multistepping, individual time-steps for the particles that are obtained by dividing the main time-step (usually $t_0/200$) by two until it is smaller than $\eta\sqrt{\epsilon(z)/a}$, where a is the local acceleration. Our standard choice is $\eta = 0.2$ and $\epsilon(z = 0)$ between 0.001 $r_{\rm vir}$ and 0.0022 $r_{\rm vir}$, ϵ is constant in physical length units since $z = 9$ and comoving before that epoch. Here we argue that the resolution limit imposed by this choice of multistepping lies well below the scale affected by finite mass resolution.

In run $D9lt$, the number of time-steps was reduced by using $\eta = 0.3$, at equal force resolution as in $D9$. Run $F9cm$ had a constant comoving softening during the entire simulation, in run $F9\,ft$ the softening is physical and the time-steps are fixed at $\Delta t = t_0\,/\,4096$ and are equal for all particles (i.e. the same numerical parameters as in F04). The density profiles are very similar (Fig. 1, Panel c); there is no significant difference above the mass resolution scale of 9 kpc. There is a small difference in the inner profile of $F9$ compared with $F9\,ft$ and $F9cm$, at large z this run has larger ϵ and therefore larger time-steps than $F9cm$. So it is possible that runs with our standard parameters have slightly shallower density profiles at the resolution limit than runs with entirely comoving softening, or runs with a sufficiently large number of fixed time-steps. However run $F9cm$ takes twice as much CPU time as run $F9$ and run $F9\,ft$ three times more, therefore we accept this compromise.

Fig. 3 shows the time-step criterion $\eta\sqrt{\epsilon(z)/a}$ as a function of radius at $z = 0$ for runs $D9$ (triangles, solid line), $D9lt$ (dashed line) $D12$ (long-dashed line) and for $F9\,ft$ (horizontal line). Particles near the cluster centre must take time-steps below $2 \times 10^{-4} t_0$, i.e. their time-steps are $t_0/200 \times 2^{-5} = t_0/6400$. According to Power et al. (2003), the resolution limit due to finite time-steps $t_{\rm ts}$ is where the circular velocity (circles) equals $15\,(\Delta t/t_0)^{5/6} t_{\rm circ}(r_{\rm vir})$ (open squares). This radius is indeed close to that where the

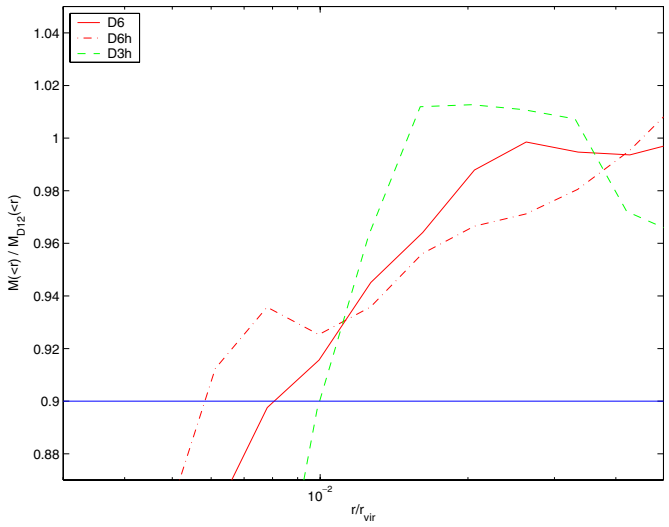

Figure 2. Ratios of the mass enclosed in low-resolution runs to the mass enclosed in the high-resolution run $D12$. By comparing runs with equal softening (smaller than one third of the convergence scale) like $D3h$ and $D6h$ one finds that the resolved radii scale like $r \propto N^{-1/3}$. A larger softening (see run $D6$) can increase the converged scales and change this scaling.

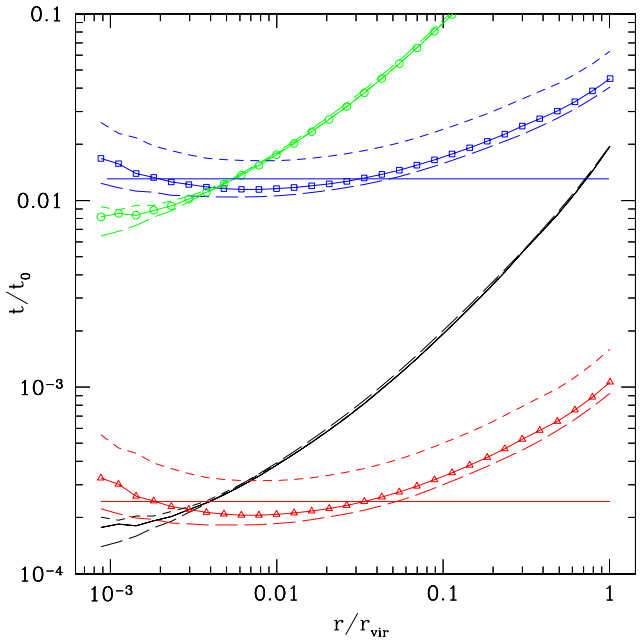

Figure 3. The triangles show the time-step criterion $\eta\sqrt{\epsilon(z)/a}$ as a function of radius for run $D9$ at $z = 0$. The dashed line is for run $D9lt$, which has $\eta = 0.3$, and the long-dashed line for run $D12$. The open squares give the 15 $(\Delta t/t_0)^{5/6} t_{\rm circ}(r_{\rm vir})$ form of Power et al. (2003), the circles are the circular orbit time-scale $2\pi\, r/v_{\rm circ}(r)$. Lines without symbols show $t_{\rm dyn}/15 = 1/(\sqrt{G\rho(<r)}15)$. The two horizontal lines are the time-steps and 15 $(\Delta t/t_0)^{5/6} t_{\rm circ}(r_{\rm vir})$ for run $F9\,ft$.

circular velocities and densities start to differ; however, for run $D9lt$ this estimate is even a bit too conservative, since the density (and also $v_{\rm circ}$) profiles of $D9lt$ and $D9$ agree down to at least 0.005 $r_{\rm vir}$. This suggest that about 15 time-steps per local dynamical time are sufficient for the simulations presented here. Other codes may require convergence conditions different from those we present in this paper. For example, F04 claim that their runs converge down to 0.003 $r_{\rm vir}$ even with only 2048 fixed time-steps, which corresponds to only eight time-steps per dynamical time at this radius.

3.2 Density profiles

In this section we present the profiles of the six high-resolution runs: $A9$, $B9$, $C9$, $D12$, $E9$, $F9cm$. The output at $z = 0$ was used, except for clusters $A9$ and $C9$, which had a recent major merger[4] and the core of the infalling cluster is at about 0.02 $r_{\rm vir}$ in $A9$ and at 0.1 $r_{\rm vir}$ in $C9$. These cores spiral in due to dynamical friction and in the 'near' future both clusters have a regular, 'relaxed' central region again. Therefore we use outputs at $z = -0.137$ (+2.1 Gyr) for run $A9$ and $z = -0.167$ (+2.6 Gyr) for $C9$.

3.3 Two-parameter fits

Fig. 4 shows the density profiles of the six different clusters. We also show best fits to functions previously proposed in the literature that have asymptotic central slopes of -1 (NFW) and -1.5 (M99). The fits are carried out over the resolved region by minimizing the mean square of the relative density differences. These two profiles have two free parameters, namely the scale radius $r_{\rm s}$ and the density at this radius $\rho_{\rm s} = \rho(r_{\rm s})$. The scale radii $r_{\rm s}$ of these best fits give the concentrations $c = r_{\rm vir}/r_{\rm s}$ listed in Table 3. The residuals are plotted in the top and bottom panels of Fig. 4 and the rms of the residuals are given in Table 3 as $\Delta_{\rm NFW}$ and $\Delta_{\rm M99}$. The residuals are quite large and show that neither profile is a good fit to all the simulations, which lie somewhere in between these two extremes.

Table 3. Density profile parameters. Δ is the root mean square of $(\rho - \rho_{\rm fit})/\rho$ for the four fitting functions used.

Run	$c_{\rm NFW}$	$\Delta_{\rm NFW}$	$c_{\rm M99}$	$\Delta_{\rm M99}$	$\gamma_{\rm G}$	$c_{\rm G}$	$\Delta_{\rm G}$	$\alpha_{\rm N}$	$c_{\rm N}$	$\Delta_{\rm N}$
$A9$	5.7	0.10	1.7	0.21	1.16	3.9	0.057	0.167	4.2	0.033
$B9$	4.2	0.16	1.5	0.13	1.29	2.1	0.083	0.141	2.6	0.093
$C9$	7.6	0.09	3.0	0.26	0.92	8.7	0.081	0.247	7.2	0.068
$D3h$	7.4	0.17	3.9	0.13	1.42	4.0	0.103	0.175	7.3	0.101
$D6h$	7.9	0.11	3.8	0.13	1.17	4.6	0.089	0.206	7.2	0.081
$D6$	7.9	0.12	3.8	0.16	1.25	5.4	0.101	0.193	7.2	0.097
$D9$	8.8	0.12	3.9	0.12	1.21	6.2	0.096	0.190	7.8	0.087
$D9lt$	8.7	0.12	3.8	0.12	1.20	6.2	0.098	0.191	7.7	0.087
$D12$	8.4	0.12	3.1	0.14	1.25	4.5	0.066	0.174	6.9	0.051
$E9$	7.4	0.12	3.0	0.10	1.25	4.5	0.072	0.176	6.2	0.069
$F9$	6.9	0.06	3.0	0.14	1.02	6.7	0.054	0.224	6.5	0.048
$F9cm$	7.3	0.06	3.1	0.14	1.10	6.2	0.055	0.212	6.6	0.057
$F9\,ft$	7.2	0.05	3.1	0.16	1.05	6.6	0.043	0.218	6.5	0.045

3.4 Three-parameter fits

Navarro et al. (2004) argue that the large residuals of NFW and M99 fits are evidence against any constant asymptotic central slope and propose a profile that curves smoothly over to a constant density at very small radii:

$$\ln(\rho_{\rm N}(r)/\rho_{\rm s}) = (-2/\alpha_{\rm N})\left[(r/r_{\rm s})^{\alpha_{\rm N}} - 1\right]. \quad (1)$$

This function gives a much better fit to the simulations, see the dash–

[4] An mpeg movie of the formation of cluster $C9$ can be downloaded from http://www-theorie.physik.unizh.ch/~diemand/clusters/

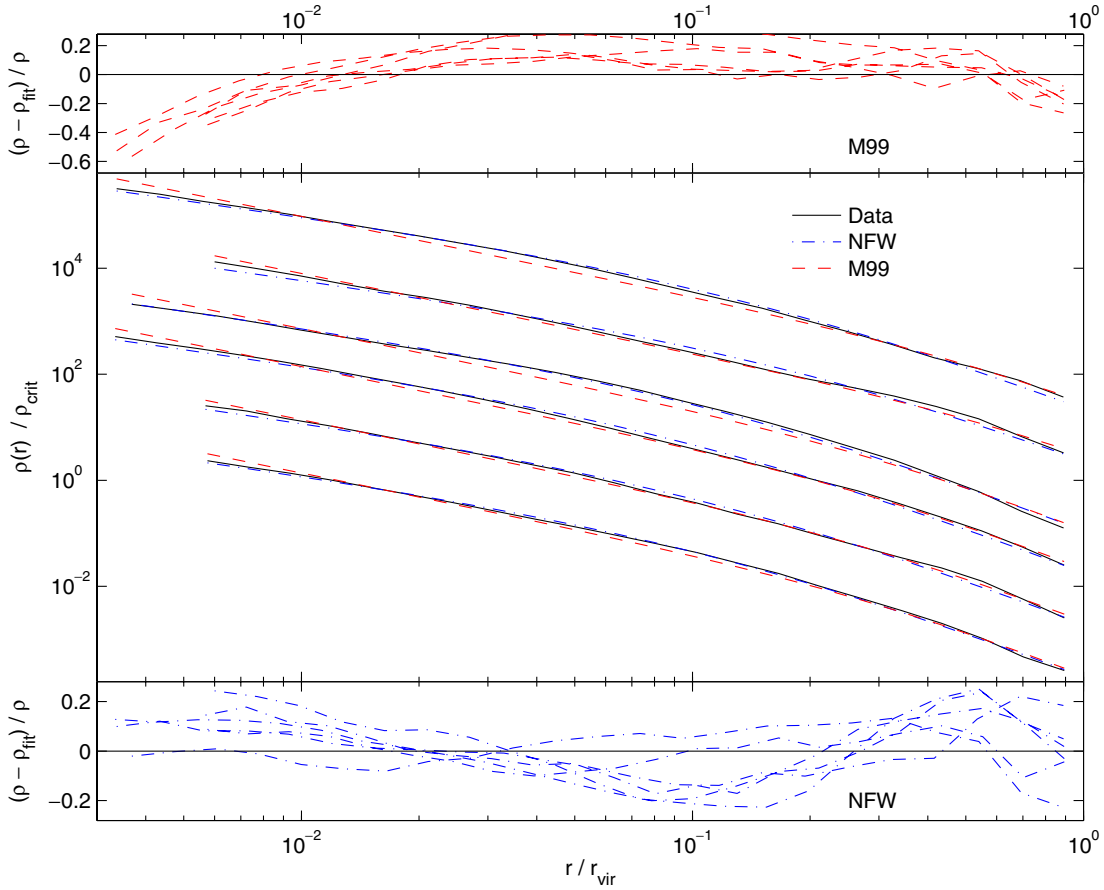

Figure 4. Density profiles of the six clusters in our sample, clusters *B* to *F* are shifted downwards for clarity. Clusters are ordered by mass form top to bottom. Profiles of cluster *A* and *C* are shown at redshifts −0.14 and −0.17, i.e. when they have reached a 'relaxed' state with one well-defined centre. Best-fit NFW and M99 profiles and residual are shown, obtained by minimizing the squares of the relative density differences.

dotted lines in Fig. 5, but this should be expected since there is an additional third free parameter α_N, while the NFW and M99 profiles only have two free parameters. α_N determines how fast the profile (1) turns away from a power law near the centre. Navarro et al. (2004) found that α_N is independent of halo mass and $\alpha_N = 0.172 \pm 0.032$ for all their simulations, including galaxies and dwarfs. The mean and scatter of our six high-resolution clusters is $\alpha_N = 0.186 \pm 0.037$. (Excluding cluster *C*9 yields $\alpha_N = 0.174 \pm 0.025$.)

We also show fits to a general $\alpha\beta\gamma$-profile (ρ_G, subscript 'G' stands for 'general') that asymptotes to a central cusp $\rho(r) \propto r^{-\gamma}$:

$$\rho_G(r) = \frac{\rho_s}{(r/r_s)^\gamma \left[1 + (r/r_s)^\alpha\right]^{(\beta-\gamma)/\alpha}}. \quad (2)$$

We fix the outer slope $\beta = 3$ and the turnover parameter $\alpha = 1$. For comparison, the NFW profile has $(\alpha, \beta, \gamma) = (1, 3, 1)$ and the M99 profile has $(\alpha, \beta, \gamma) = (1.5, 3, 1.5)$. We fit the three parameters γ, r_s and ρ_s to the data and find that this cuspy profile also provides a very good fit to the data. The best-fit values and rms residual are listed in Table 3 and we find a mean slope of $\gamma = 1.16 \pm 0.14$.

Using a sharper turnover $\alpha = 1.5$ makes the fits slightly worse (the average of Δ_G is about 20 per cent larger) and the best-fit inner slopes are somewhat steeper at $\gamma = 1.31 \pm 0.11$.

The fitting functions (1) and (2) fit the measured density profiles very well over the whole resolved range. Function (1) is even a relatively good approximation *below* the resolved scale: for example if one is extremely optimistic about $r_{resolved}$ in run *D*6 and uses $r_{resolved} = 2.8$ kpc instead of 13.5 kpc one gets $\alpha_N = 0.0203$, $c_N = 7.1$ and $\Delta_N = 0.127$, while the generalized fit is now clearly worse: $\gamma_G = 0.99$, $c_G = 3.6$ and $\Delta_G = 0.216$. Also note that the residuals near $r_{resolved}$ are very small or positive for (1), i.e. the measured density is as large as the fitted value. But at $r_{resolved}$ it is possible that the measured density is slightly too low since in this region the numerical limitations start to play a role. If extrapolation beyond the converged radius is necessary it is not clear which profile is a safer choice. We agree with Navarro et al. (2004) that all simple fitting formulae have their drawbacks, that direct comparison with simulations should be attempted whenever possible and that much higher-resolution simulations are needed to establish (or exclude) that CDM haloes have divergent inner density cusps (as predicted in Binney 2003).

3.5 Maximum inner slope

The results from the last section suggest that profiles with a central cusp in the range $\gamma = 1.16 \pm 0.14$ provide a good approximation to the inner density profiles of ΛCDM haloes. But fig. 4 in Navarro et al. (2004) seems to exclude our mean value for more than half of their cluster profiles. This is not totally inconsistent, it is only a hint of a mild discrepancy that we will try to explain: in principle the mass inside the converged radius limits the inner slope: $\gamma_{max} = 3[1 - \rho(r)/\overline{\rho(,r)}]$. This is true if both the density and the cumulative density are correct down to the resolved

scale. But up to now the central density of a simulated profile always increased with better numerical resolution, so it is likely that also today's highest-resolution simulations underestimate the dark matter density near the centre. This means that cumulative quantities like $v_{\rm circ}(r)$, $\overline{M(<r)}$ and $\overline{\rho(<r)}$ tend to be too low even at radii where the density has converged. The converged radii used in Navarro et al. (2004) are close to the radius where the circular velocity is within 10 per cent of a higher-resolution run, while the density converges further in at about 0.6 $r_{\rm conv}$ (H03). If we assume that this is also true for their highest-resolution runs then $\overline{\rho(<r)} \propto v_{\rm circ}(r)^2$ is up to 20 per cent too low, while the error in $\rho(r)$ is much smaller. This raises the values for $\gamma_{\rm max}$ by about $0.2 \sim 0.3$ and our mean value $\gamma = 1.16$ is not excluded by any of their clusters anymore. If the convergence with mass resolution is not as fast as $r_{\rm conv} \propto N^{-0.45}$ but rather $r_{\rm conv} \propto N^{-1/3}$, see Section 3.1, then the maximum inner slopes could have even larger errors.

4 COMPARISON WITH OTHER GROUPS

Recently, several groups have published simulations of dark matter clusters in the concordance cosmological model. These authors kindly supplied their density profiles and we show the comparison here. F04 simulated four ΛCDM clusters with 7 to 26 million particles using a Treecode and the GRAPE hardware. These authors also used the GRAFIC 2 software (Bertschinger 2001) to generate their initial conditions. H03 and Navarro et al. (2004) presented eight clusters resolved with up to 1.6 million particles within r_{200} simulated with the GADGET code (Springel, Yoshida & White 2001); the method used to generate the initial conditions is described in Power et al. (2003). T04 simulated six clusters with up to 0.8 million particles within r_{180} using the adaptive refinement tree code ART (Kravtsov, Klypin & Khokhlov 1997) and a technique for setting up multi-mass initial conditions described in Klypin et al. (2001). W04 present a cosmological simulation without re-simulation of refined regions, i.e. constant mass resolution (1024^3 particles in a 320 h^{-1} Mpc box). The four most massive clusters in this cube are resolved within 0.5 to 0.9 million particles. This simulation was performed with a Tree–Particle–Mesh (TPM) code (Bode & Ostriker 2003) with a softening of 3.2 h^{-1} kpc.

In Fig. 6 we show these data along with the new simulations presented in this paper. We plot the density profiles and the logarithmic slopes of the clusters all normalized at the radius such that the circular velocity curve peaks $r_{\rm Vcmax}$ and to $\overline{\rho(<r_{\rm Vcmax})}$. This corresponds to the radius at which $\mathrm{d}\log\rho/\mathrm{d}\log r = -2$. We plot the curves to the 'believable' radius stated by each group and down to about 0.01 $r_{\rm vir}$ for W04.

The density profiles are reassuringly similar. Furthermore, the scatter is small, roughly ± 0.15 in the logarithmic gradient at small radii (0.01–0.5 $r_{\rm Vcmax}$). Table 4 lists the measured slopes at different radii. There is no value at 3 per cent $r_{\rm Vcmax}$ for the cluster from

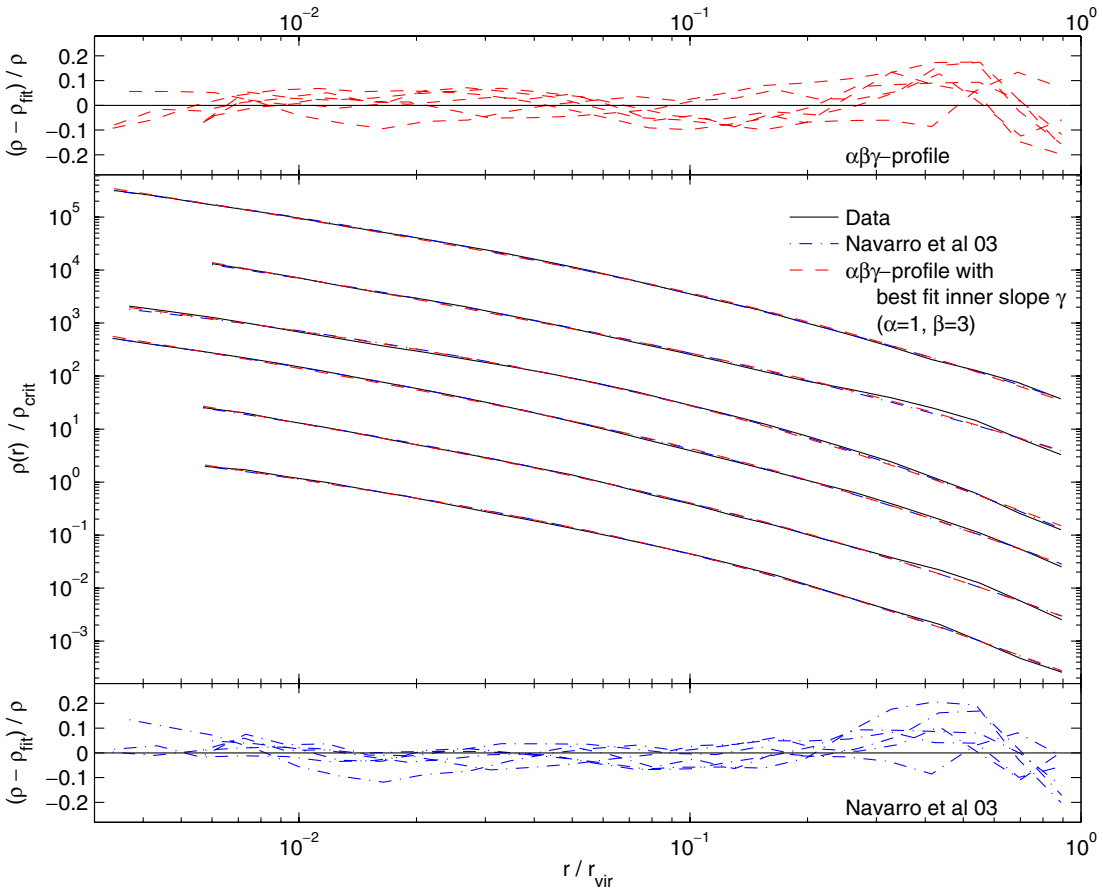

Figure 5. Same as Fig. 4, but with fitting functions that have one additional free parameter. The dash–dotted lines show the profile (1) proposed by (Navarro et al. 2004). The dashed lines show a general $\alpha\beta\gamma$-profile (2). We fitted the inner slope γ to the data and used fixed values for the outer slope $\beta = 3$ and turning parameter $\alpha = 1$. $\gamma = 1$ corresponds to the NFW profile. The fit parameters and rms of the residuals are given in Table 3.

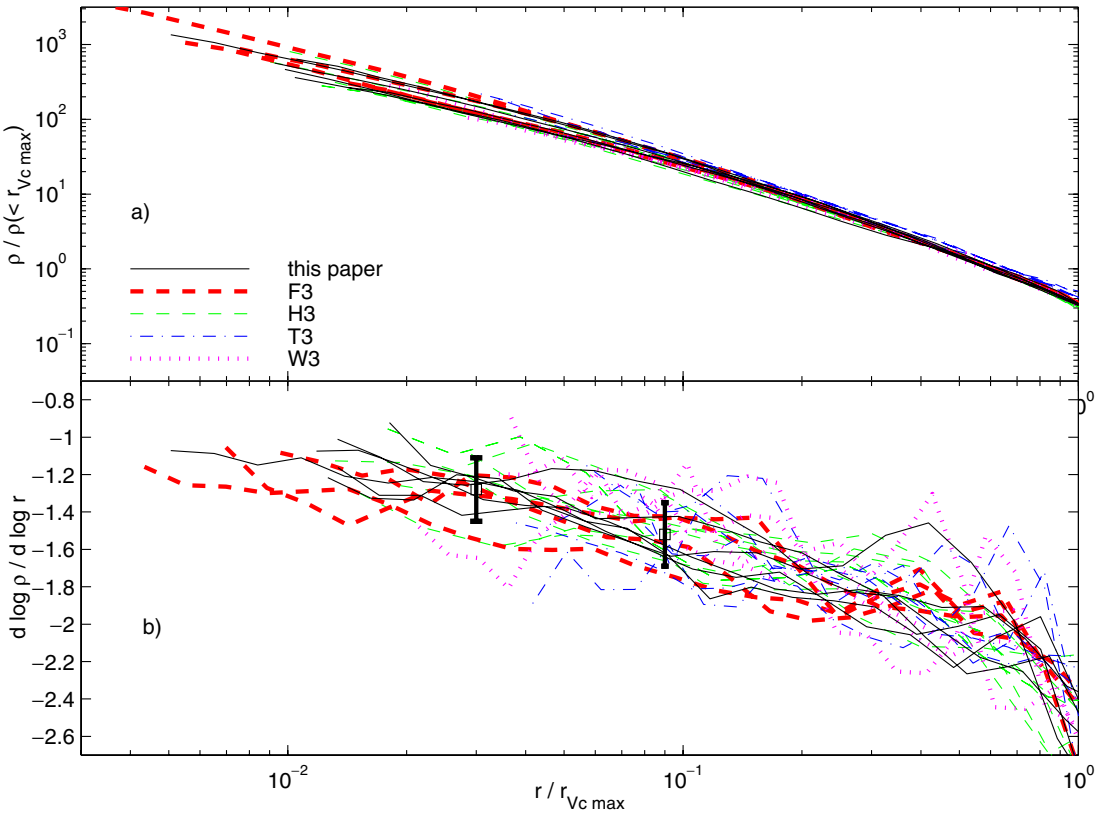

Figure 6. Panel (a): density profiles of cluster simulated by different groups normalized to the radius were the circular velocity peaks $r_{\rm Vcmax}$ and to $\overline{\rho(<r_{\rm Vcmax})}$: six clusters from this paper (solid lines), four from F04 (thick-dashed lines), eight from H03 (thin-dashed lines), six from T04 (dash–dotted lines), four from W04 (dotted lines). Despite the different codes, parameters and initial conditions used, the results are very similar. Panel (b): logarithmic slope for the profiles from (a). Points with error bars give the averages at 0.03 and 0.09 $r_{\rm Vcmax}$ and a scatter of 0.15 (see Table 4).

T04 and W04 because this is below their quoted resolution limit. Most values agree within the scatter, the profiles from T04 are steeper when compared at 0.01 and 0.03 $r_{\rm vir} \equiv r_{98.4}$, but within the scatter at 3 per cent $r_{\rm Vcmax}$. This could be due to different halo selection. The majority of their clusters are not isolated but in close pairs or triplets. In a close pair the density falls slower with radius to 98.4 $\rho_{\rm crit}$, so $r_{\rm vir} \equiv r_{98.4}$ is further out as in a isolated cluster with similar inner profile. Among the samples of isolated clusters (F04; H03; W04 and our clusters) there is a small trend at 0.01 $r_{\rm vir}$ towards steeper slopes with better mass resolution.

5 SUMMARY

We have carried out a series of six very-high-resolution calculations of the structure of cluster mass objects in a hierarchical universe. The clusters contain up to 25 million particles and have force softening as small as 0.1 per cent $r_{\rm vir}$.

Table 4. Logarithmic slopes (absolute values) of our six high-resolution cluster density profiles. Line (a) gives the averages and scatter. (b) and (c) are average slopes from other groups (see text for details).

	1 per cent $r_{\rm vir}$	3 per cent $r_{\rm vir}$	3 per cent $r_{\rm Vcmax}$	9 per cent $r_{\rm Vcmax}$
*A*9	1.22	1.36	1.24	1.64
*B*9	1.33	1.43	1.21	1.63
*C*9	1.24	1.21	1.25	1.26
*D*12	1.28	1.54	1.32	1.58
*E*9	1.31	1.44	1.41	1.62
*F*9*cm*	1.19	1.47	1.22	1.43
(a) *A*–*F*	1.26 ± 0.05	1.41 ± 0.11	1.28 ± 0.08	1.53 ± 0.15
(b) F04	1.25 ± 0.05	1.52 ± 0.06	1.33 ± 0.15	1.54 ± 0.15
(c) H03	1.18 ± 0.13	1.38 ± 0.14	1.23 ± 0.17	1.50 ± 0.14
(d) T04	1.50 ± 0.14	1.79 ± 0.07	–	1.56 ± 0.12
(e) W04	1.11 ± 0.04	1.41 ± 0.13	–	1.35 ± 0.06
avg (a–e)	1.26	1.50	–	1.49
avg (a–c)	1.23	1.44	1.28	1.52

A convergence analysis demonstrates that for our Treecode with our integration scheme, the radius beyond which we can trust the density profiles scale according to the mean interparticle separation. In the best case we reach a resolution of about 0.3 per cent $r_{\rm vir}$.

Neither of the two-parameter functions, the NFW and M99 profiles, are very good fits over the whole resolved range in most clusters. One additional free parameter is needed to fit all six clusters: the asymptotically flat profile from Navarro et al. (2004) and an NFW profile with variable inner slope provide much improved fits. The best-fit inner slopes are $\gamma = 1.16 \pm 0.14$. *Below* the resolved radius the two fitting formulas used are very different. Future simulations with much higher resolution will show which one (if either) of the two is still a good approximation on scales of 0.1 per cent $r_{\rm vir}$ and smaller.

We compare our results with simulations from other groups who used independent codes and initial conditions. We find a good agreement between the cluster density profiles calculated with different algorithms. From 0.03–0.5 $r_{\rm Vcmax}$ the scatter in the profiles is nearly constant and equal to about 0.17 in logarithmic slope. At one per cent of the virial radius (defined such that the mean density within $r_{\rm vir}$ is 178 $\Omega_{\rm M}^{0.45} \rho_{\rm crit} = 98.4\ \rho_{\rm crit}$) the slope of the density profiles is 1.26 ± 0.16.

ACKNOWLEDGMENTS

We are grateful to Toshiyuki Fukushige, Eric Hayashi, Argyro Tasitsiomi and Paul Bode for providing the density profile data from their cluster simulations. We thank the Swiss Centre for Scientific Computing in Manno for computing time to generate the initial conditions for our simulations. All other computations were performed on the zBox supercomputer at the University of Zurich. JD is supported by the Swiss National Science Foundation.

REFERENCES

Baertschiger T., Joyce M., Sylos Labini F., 2002, ApJ, 581, L63
Bertschinger E., 2001, ApJS, 137, 1
Bode P., Ostriker J. P., 2003, ApJS, 145, 1
Binney J., 2004, MNRAS, 350, 939
Binney J., Knebe A., 2002, MNRAS, 333, 378
Calcáneo-Roldán C., Moore B., 2000, Phys. Rev. D, 62, 123005
Davis M., Efstathiou G., Frenk C. S., White S. D. M., 1985, ApJ, 292, 371
de Blok W. J. G., Bosma A., 2002, A&A, 385, 816
de Blok W. J. G., McGaugh S. S., Bosma A., Rubin V. C., 2001a, ApJ, 552, L23
de Blok W. J. G., McGaugh S. S., Rubin V. C., 2001b, AJ, 122, 2396
Diemand J., Moore B., Stadel J., Kazantzidis S., 2004, MNRAS, 348, 977
Dubinski J., Carlberg R. G., 1991, ApJ, 378, 496
Eke V. R., Cole S., Frenk C. S., 1996, MNRAS, 282, 263
Flix J., Martinez M., Prada F., 2004, preprint (astro-ph/0401511)
Fukushige T., Makino J., 1997, ApJ, 477, L9
Fukushige T., Makino J., 2001, ApJ, 557, 533
Fukushige T., Kawai A., Makino J., 2004, ApJ, 606, 625 (F04)
Ghigna S., Moore B., Governato F., Lake G., Quinn T., Stadel J., 1998, MNRAS, 300, 146
Ghigna S., Moore B., Governato F., Lake G., Quinn T., Stadel J., 2000, ApJ, 544, 616
Hayashi E. et al., 2003, preprint (astro-ph/0310576) (H03)
Jing Y., Suto Y., 2000, ApJ, 529, L69
Jing Y., Suto Y., 2002, ApJ, 574, 538
Klypin A., Kravtsov A. V., Bullock J. S., Primack J. R., 2001, ApJ, 554, 903
Knebe, A., Kravtsov A. V., Gottlöber S., Klypin A. A., 2000, MNRAS, 317, 630
Kravtsov A. V., Klypin A. A., Khokhlov A. M., 1997, ApJ, 111, 73
McGaugh S. S., Rubin V. C., de Blok W. J. G., 2001, AJ, 122, 2381
Moore B., Governato F., Quinn T., Stadel J., Lake G., 1998, ApJ, 499, L5
Moore B., Quinn T., Governato F., Stadel J., Lake G., 1999, MNRAS, 310, 1147 (M99)
Moore B., 2001, in Martel H., Wheeler J., eds, AIP Conf. Proc. 586, Relativistic Astrophysics: 20th Texas Symp. Am. Inst. Phys., New York, p. 73
Navarro J. F., Frenk C. S., White S. D. M., 1996, ApJ, 462, 563 (NFW)
Navarro J. F. et al., 2004, MNRAS, 349, 1039
Peebles P. J. E., 1970, AJ, 75, 13
Power C., Navarro J. F., Jennkins A., Frenk C. S., White S. D. M., 2003, MNRAS, 338, 14
Reed D., Governato F., Verde L., Gardner J., Quinn T., Stadel J., Merritt D., Lake G., 2003, preprint (astro-ph/0312544)
Sand D. J., Treu T., Smith G. P., Ellis R. S., 2004, ApJ, 604, 88
Spergel D. N. et al., 2003, ApJS, 148, 175
Springel V., Yoshida N., White S. D. M., 2001, New Astron., 6, 79
Stadel J., 2001, PhD thesis, Univ. Washington
Swaters R. A., Madore B. F., van den Bosch F. C., Balcells M., 2003, ApJ, 583, 732
Tasitsiomi A., Kravtsov A. V., Gottlober S., Klypin A. A., 2004, ApJ, 607, 125 (T04)
Wambsganss J., Bode P., Ostriker J. P., 2004, ApJ, 607, 125 (W04)
Warren M. S., Quinn P. J., Salmon J. K., Zurek W. H., 1992, ApJ, 399, 405
Weekes T. C. et al., 2002, Astropart. Phys., 17, 221

This paper has been typeset from a TEX/LATEX file prepared by the author.